Optimal Trajectory Planning for Mitigated Motion Sickness: Simulator Study Assessment

Vishrut Jain, Sandeep Suresh Kumar, Georgios Papaioannou, Riender Happee, and Barys Shyrokau

***Abstract*— In the transition from partial to high automation, occupants will no longer be actively involved in driving. This will allow the use of travel time for work or leisure, where high comfort levels preventing motion sickness are required. In this paper, an optimal trajectory planning algorithm is presented in order to minimise motion sickness in automated vehicles. A predefined path is provided as an input to the algorithm, to generate an optimal path with limited lateral deviation and the corresponding optimal velocity profile, for the minimisation of motion sickness. An optimal control problem is formulated with a cost function combining both motion sickness and travel time. For a sickening curvy road, the algorithm reduced the motion sickness dose value (MSDV) up to 52% depending on the allowed lateral deviation and the weighting on travel time. The efficacy of the proposed algorithm has been evaluated via human-in-the-loop experiments using a moving-base driving simulator. Motion cueing parameters were selected to optimally transmit the sickening stimuli resulting in close to full vibration transmission above 0.2 Hz. During the experiment, the participants were asked to rate their experience based on the standard MIsery SCore ratings. According to these, sickness levels were reduced on average by 65% with reduced motion sickness in all 16 participants.**

***Index Terms*— Automated driving, motion sickness, optimal control, driving simulator, motion planning.**

I. Introduction

AUTOMATED vehicles (AVs) are projected to be safer than manual driving, efficient in terms of traffic flow and cheaper in the cost of transportation [1]. In fact, by 2050, AVs are predicted to have a market share of about 50% of all on-road vehicle sales [2]. The wide adoption of this disruptive innovation could create a massive impact on public mobility. With higher automation levels, the occupants are not required to be actively involved in driving. This will enable the productive use of travel time for work or leisure [3], an appeal that is a major driving force behind the adoption of AVs by the public [4]. However, when using the time inside the vehicle for non-driving tasks, where there is limited awareness about the surrounding of the AV, the ride experience and comfort for the passengers will deteriorate, making them more prone to motion sickness (MS) [5]. Hence, high levels of comfort should be achieved within AVs, preventing MS and excessive body motion, both of which can lead to discomfort. In this direction, the "AV driving style" should not only be carefully designed, but also experimentally tested to check the comfort perceived by occupants, when exposed to this driving style.

This work aims to reduce sickening stimuli by planning the vehicle motion around a predefined path, using optimal control, and thus mitigating its sickening effects on passengers in automated vehicles. While generating an optimal path that is more suitable for mitigating MS, the algorithm also searches the optimal velocities for different sections of the path as well as deceleration and acceleration profiles negotiating curves. The effectiveness of the proposed algorithm in reducing MS has been assessed via human-in-the-loop experiments. The occupants of an AV are expected to be involved in non-driving tasks, without the visual awareness of the surrounding environment. Therefore, in the conducted experiment, the participants performed a non-driving task in absence of visual cues related to the road. This ensures participants' exposure to an environment similar to that of an AV and eliminates any additional sickening effects of the sensory conflicts arising through visual cues.

The contributions of the paper are as follows:

- We use a non-linear bicycle model as the internal model for the optimal control problem (OCP), instead of the commonly used point mass model which oversimplifies the dynamics of a real vehicle.
- We use a standardized motion sickness metric (MSDV) instead of solely minimising jerk, acceleration or both. At the same time, we not only consider this metric for the current prediction horizon, but also take into account travel time and the accumulation of sickness across the entire journey.
- We perform a first ever human-in-the-loop experimental validation to subjectively validate an MS mitigation algorithm, using a moving-base driving simulator. Motion cueing parameters were selected to optimally transmit the sickening stimuli resulting in close to full vibration transmission above 0.2 Hz. Results confirm the effectiveness of the proposed trajectory planning in reducing motion sickness.

The paper is organized as follows: section II discusses the existing works in the domain of driving comfort and MS reduction; section III provides the details of the proposed

Manuscript received 30 April 2022; revised 18 October 2022, 19 January 2023, and 13 March 2023; accepted 17 May 2023. Date of publication 12 June 2023; date of current version 4 October 2023. This work was supported by Toyota Motor Europe. The Associate Editor for this article was X. Li. *(Corresponding author: Vishrut Jain.)*

This work involved human subjects or animals in its research. Approval of all ethical and experimental procedures and protocols was granted by the Human Research Ethics Committee of TU Delft, The Netherlands, under Application No. 1675.

The authors are with the Department of Cognitive Robotics, Delft University of Technology, 2628 CD Delft, The Netherlands (e-mail: v.j.jain@tudelft.nl; b.shyrokau@tudelft.nl).

Digital Object Identifier 10.1109/TITS.2023.3281724

algorithm and formulates the optimal control problem (OCP); section IV presents the experiment design for the validation of the proposed algorithm; section section V illustrates the results of the experiments; then, section VI follows, where the results are analysed and their significance is discussed; finally, conclusions are extracted in section VII.

II. Existing Studies

Various geometric, constraint and optimisation-based motion control methods have been investigated to enhance occupants' comfort in automated driving [6]. Geometric-based and heuristic-based methods mainly address path generation, while optimal control-oriented methods focus on generation of a feasible trajectory, by assigning a velocity profile over a pre-defined path.

Geometrical methods employ clothoids, bezier curves, and others to generate a smooth path or to smoothen an existing one [7], [8], [9]. In addition to the design of the path, quintic bezier curves have been used to assure smooth and continuous velocity and acceleration profiles [10]. Constraint-based methods set upper comfort limits to acceleration and jerk [11], while iterative numerical methods that restrict vehicle acceleration and jerk within a comfortable range have also been explored [12]. The restrictions are set according to comfort limits. Then, the solution is searched for the vehicle to have the maximum allowable jerk according to the comfort range. This search runs in a loop, where if the solution fails or is unachievable, the jerk values are reduced and a new search starts until a feasible solution is achieved. Numerical iterative methods for minimum time velocity planning utilize the upper limits of the defined jerk range to obtain minimum travel time [13]. However, constraint-based methods predominantly work in the defined upper limits to plan the motion, which may lead to accumulated discomfort over long periods.

Although the restriction of jerk and acceleration, using numerical methods, demonstrates positive effects on motion comfort, a more common approach is the use of optimisation for motion planning. By applying cost functions for the translation of vehicle motion to perceived comfort, higher levels of comfort can be obtained in comparison to methods only constraining acceleration, velocity, and jerk. Motion planning has been conducted minimising the lateral and longitudinal accelerations using optimisation [14]. The addition of journey time in the cost function, to make the algorithm time efficient and comfortable has also been explored [15]. Trajectory planning has also been conducted using a combination of jerk, acceleration, and travel time as the cost function to be minimised [16]. Additionally, velocity and yaw rate inclusion in the cost function has been analysed [17]. Moreover, several studies explore combinations of the above-mentioned strategies, to achieve a more comfortable ride. Optimisation over a smooth path for the planning of vehicle motion has been investigated using geometric curves [18], [19]. Where a path is first smoothed using quintic bezier curves, an optimal velocity planning is then run over this path. These studies focus on motion comfort through minimisation of acceleration and jerk over a wide frequency range. To address motion sickness, low-frequency motion requires particular attention and different approaches have been considered.

Emphasising MS mitigation, use of vibrational cueing in the seat, to generate anticipation of the future motion of the vehicle, has been explored [20]. Vibrational cues resulted in lower MS levels for the participants of the study. However, no MS model was involved in this work. Only a few studies use MS models to plan vehicle motion. A vehicle-following algorithm has been designed, which minimises the sensory conflict obtained through the 6-DoF Subjective Vertical Conflict model [21]. The use of optimisation to obtain velocity profiles to reduce MS is explored [22]. The effectiveness of MS mitigation was gauged numerically, comparing the respective motion sickness incidence (MSI) obtained using different cost functions. The results showed that adaptive MS cost was the most effective in MS mitigation; however, acceleration cost showed very similar results, with a significantly lower computational expense. This indicates that the acceleration cost is a promising candidate for MS mitigation. However, in this study, the lateral dynamics were simplified using a point mass vehicle model. The model only considered longitudinal jerk as the input, the lateral accelerations were calculated using longitudinal velocity and road curvature. Similarly, an optimal velocity profiling architecture using optimal control-oriented methods is proposed using Motion Sickness Dose Value (MSDV) as a cost function for minimisation [23]. Such an approach allowed deviation of the vehicle from the predefined path and showed substantial MSDV reduction when more lateral deviation is allowed. However, the adopted point mass model does not accurately represent the dynamics of a real vehicle, and thus the algorithm may provide sub-optimal results. A frequency-shaping approach to motion planning has also been proposed, which uses frequency-weighted MSDV as a cost function in the OCP framework [24]. This approach reduced acceleration in the frequency range which provokes motion sickness to the occupants. However, the effectiveness of the algorithm wasn't confirmed using any human-in-the-loop experiment. Moreover, the vehicle model was highly simplified. At the same time, the journey time was not included in the cost function, and the motion planner could conclude in long rides that can decrease the occupant's satisfaction. Our proposed algorithm considers a more sophisticated vehicle model, which allows the algorithm to look for a more suitable path for mitigating MS. The algorithm also considers journey time minimisation along with MSDV to reach the destination within a desirable time, illustrating the trade-off between comfort and travel time. Additionally, our study involved human-in-the-loop driving simulator experiments, which demonstrated the effectiveness of the algorithm in mitigating MS.

Motion sickness modelling is known to require objective measures capturing low-frequency motion and representing sickness accumulation over longer time periods [25]. This work accounts for the accumulation of motion sickness over longer periods. This is achieved by optimizing motion over the shifting-control horizon window N_c, using the current MSDV as an initial state representing MS accumulation due to past motion. Finally, results are presented recalculating MSDV over the entire trip. Furthermore, to the best of authors' knowledge,

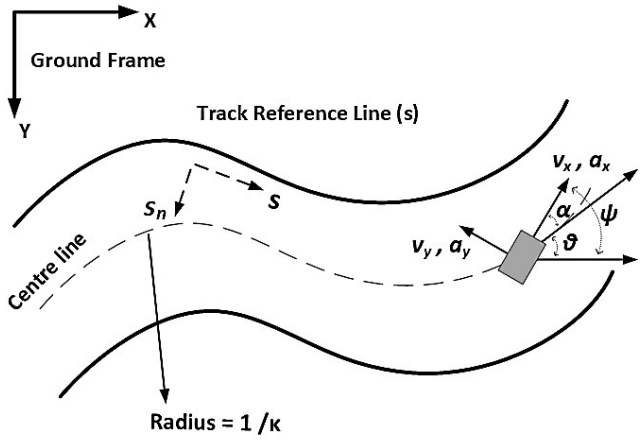

Fig. 1. Depiction of the vehicle on the road.

the proposed algorithms to date have been analysed only via simulation. However, human beings are differently susceptible to motion sickness, and no single metric represents this individuality accurately and hence can't effectively evaluate the efficacy of such algorithms in mitigating motion sickness. Therefore, experimental validation with human participants was performed, using a driving simulator.

III. Optimal Control Strategy

This section describes our novel AV trajectory planning algorithm for MS mitigation. The problem is defined as an OCP applied to driving on a predefined path without other road users. The cost functions are considered to represent MS accumulation and journey time. Constraints secure the feasibility of the optimal solutions.

A. Vehicle Model

A 3-DOF nonlinear bicycle model with linear tyre model is used to represent the vehicle dynamics. The modeling equations are given in vehicle's frame of reference. Figure 1 depicts the variable nomenclature used in the modeling. The vehicular accelerations (a_x and a_y), and yaw rate (r) are defined as:

$$\dot{v}_x = a_x + v_y r \tag{1}$$

$$\dot{v}_y = -\left(\frac{C_{\alpha f} + C_{\alpha r}}{m v_x}\right) v_y + \left(\frac{l_r C_{\alpha r} - l_f C_{\alpha f}}{m v_x} - v_x\right) r + \frac{C_{\alpha f}}{m}\delta \tag{2}$$

$$\dot{r} = \left(\frac{l_r C_{\alpha r} - l_f C_{\alpha f}}{I_z v_x}\right) v_y \tag{3}$$

where v_x and v_y are the longitudinal and lateral velocities respectively; δ is the road wheel angle; $C_{\alpha f}$ and $C_{\alpha r}$ are the front and rear cornering stiffness respectively; m is the mass of the vehicle; I_z is the inertia moment of vehicle about vertical axis; l_f and l_r are the distances of the vehicle centre of gravity from the front and the rear axles, respectively.

The road is defined using curvilinear coordinates. The road co-ordinates and the road heading angle θ are described by:

$$\frac{dx}{ds} = cos\theta; \quad \frac{dy}{ds} = sin\theta; \quad \frac{d\theta}{ds} = \kappa(s); \tag{4}$$

where κ is the road curvature. Additionally, the distance covered by the vehicle (s), the lateral deviation of the vehicle from the lane center (s_n) and the deviation of the vehicle heading angle from the road heading angle ($\alpha = \psi - \theta$) are given as:

$$\dot{s} = \frac{v_x cos\alpha - v_y sin\alpha}{1 - s_n \kappa(s)} \tag{5}$$

$$\dot{s}_n = v_x sin\alpha + v_y cos\alpha \tag{6}$$

$$\dot{\alpha} = r - \dot{s}\kappa(s) \tag{7}$$

B. Optimal Control Problem

The problem is to find a reference trajectory for the vehicle to follow. It is assumed that the vehicle shall approximately follow a predefined path from an initial position (s_0) to a final position (s_f). As objective a weighted combination of MS metric and travel time is considered, to reduce the sickening effect of the ride and incorporate time efficiency as well.

1) Motion Sickness Metric: MSDV is a metric quantifying motion sickening accumulation in time as defined in ISO 2631 standard [26]. This metric accounts for the frequency related sickening stimuli by weighting the acceleration for different frequency ranges, as MS depends on the frequency of motion an individual is subjected to [27]. The metric is defined as:

$$MSDV = \sqrt{\int_0^T [a_{x,w}(t)]^2 dt} + \sqrt{\int_0^T [a_{y,w}(t)]^2 dt} \tag{8}$$

where $a_{x,w}(t)$ and $a_{y,w}(t)$ are frequency weighted accelerations in longitudinal and lateral directions in time domain; t, dt is the time increment, and T is the exposure time. The weighting curve constitutes of a 0.02-0.63 Hz bandpass filter based on [28]. The weightings for the longitudinal and lateral acceleration are assumed to be the same in this study, as there is no clear guideline in the literature for the longitudinal filters.

2) Cost Function: The cost function for the prediction horizon is given by:

$$J_c = \sum_{i=0}^{N_c} w_m MSDV_i + w_t T_i \tag{9}$$

where w_m and w_t are the weighting coefficients for MSDV and travel time respectively, and N_c is the length of the prediction horizon.

As travel time is one of the criteria to be minimised, the problem is solved in space domain instead of time domain. The whole state space is converted from time domain to space domain using the relation given in Equation 10.

$$\frac{dp}{ds} = p' = \frac{dp}{dt}\frac{dt}{ds} = \dot{p}\dot{s}^{-1} \tag{10}$$

where p is the time dependent variable represented in space domain instead of time. Thus the OCP horizon is expressed in distance instead of time.

The travel time can be represented as:

$$T = \int_0^T dt = \int_{s_0}^{s_f} \frac{dt}{ds} ds = \int_{s_0}^{s_f} \dot{s}^{-1} ds \tag{11}$$

For the dynamics of the problem as defined in subsection III-A, the feasibility and continuity of the acceleration and road wheel angle should be considered. Thus, their time derivatives i.e. jerk, J_x and rate of road wheel angle, d_δ, are chosen as the control inputs. Hence, the vehicle model is described as:

$$x'_v = f_v(x_v, u) \tag{12}$$

where $x_v = [v_x \ v_y \ r \ s_n \ \alpha \ a_x \ \delta]^T$ are the vehicle states, and $u = [J_x \ d_\delta]$ are the control inputs.

The constraints on the state s_n are kept non zero allowing some deviation from the predefined path (lane centre line) to obtain a further reduction in MS levels. Along with the constraints on the states of the vehicle model, an additional constraint representing the friction circle is added to the problem, to ensure that the vehicle remains in its functional limits. The friction circle defines the maximum acceleration that the vehicle can attain due to limited friction between road and the tyre. This constraint is defined as:

$$\sqrt{a_x^2 + a_y^2} \leq \mu m g \tag{13}$$

where μ is the road friction coefficient and g is the acceleration due to gravity.

The OCP is formulated as:

$$\min_{u \in U} \quad J_c \tag{14}$$

$$s.t. \ x'_v = f_v(x_v, u) \tag{15}$$

$$\phi(x_v, u) \leq 0 \tag{16}$$

$$b\left(x\left(s_0\right), x\left(s_f\right)\right) = 0 \tag{17}$$

The dynamics of the system are represented in Equation 15 using equality constraints, defined by the function f_v. The parameter ϕ in Equation 16 defines/represents the constraints on the vehicle limits (acceleration, velocities, etc.) including the friction circle constraint represented in Equation 13. Lastly, function $b(x(s_0), x(s_f)))$ in Equation17 defines/represents the boundary conditions for the vehicle i.e. the initial states and the final states of the vehicle.

The optimal driving style obtained by the algorithm will hereon be referred to as '*Motion sickness mitigation drive*' (MSM drive).

The optimisation is conducted with the ForcesPro solver [29], using sequential quadratic programming. The optimisation was run for the whole road but due to the long length of the road, a sliding window (where the optimisation is solved as smaller OCPs, sliding the prediction horizon forward by a defined number of steps over the complete horizon) has been applied to reduce the computational load on the solver. The detailed settings can be referred to in Appendix C. The shifting-control horizon window N_c was chosen to be 100 steps (100 m) to reduce the computation time. It should be emphasised that as a sliding window approach has been used, MSDV is added as a state during the optimisation. This allows us to initialise MSDV with its current value, which ensures that accumulation of the sickness dose over the entire journey is considered. The number of solver iterations is chosen to be 2000, to ensure convergence and avoid sub-optimal solutions.

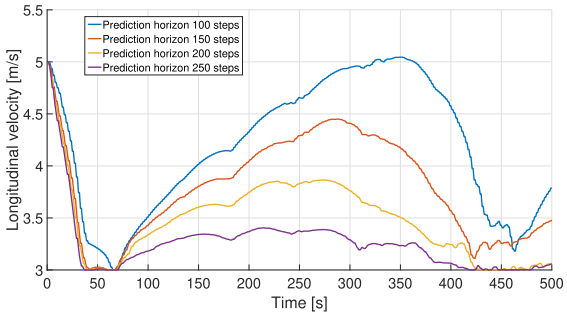

Fig. 2. Velocity profiles for horizon lengths of 100, 150, 200 and 250 steps respectively.

TABLE I

OBTAINED TRAVEL TIME, MSDV AND THE COMPUTATION TIME FOR DIFFERENT PREDICTION HORIZON LENGTHS

Prediction horizon	Travel time [s]	MSDV [m/s$^{1.5}$]	Computation time [s]
100 steps	122	6.97	39
150 steps	133	6.00	54
200 steps	144	5.58	69
250 steps	154	5.47	79

The optimisation has been performed on Intel(R) Xeon(R) W-2223 CPU @3.60GHz with 32GB RAM.

With the above-mentioned settings, the computation time for the algorithm is reported. The time taken for the algorithm to arrive at a solution varies based on the complexity of the road and the initial guess provided to the algorithm. To analyse the effect of the length of the shifting-control horizon, simulations were conducted considering 100, 150, 200 and 250 steps as prediction horizon respectively (for even larger horizons ForcesPro failed to converge). The simulations were conducted for a reduced drive with a length of 500 steps, keeping all the conditions apart from the prediction horizon the same. The obtained results are presented in Figure 2. Comparing the different horizons, a similar trend in acceleration and deceleration is observed, however, there is a difference in the resultant velocity profile. This behaviour aligns with the expectation. For a smaller prediction horizon, the algorithm takes more aggressive actions due to the lack of information about the future. The obtained travel time and MSDV at the end of the 500 m (500 step) journey, along with the time taken for the OCP solution is reported in Table I.

This indicates that reducing the size of the prediction horizon makes the solution much faster. Thus a smart choice of prediction horizon should be made for obtaining desired MS reduction and at the same time keeping the algorithm computationally inexpensive.

As can be observed from Table I, using the above-mentioned PC configuration, for a 122 second simulation the algorithm takes a simulation time of 39 seconds. This corresponds to a real-time factor of 0.32. Thus, the algorithm is real-time implementable, as it takes less computation time than the real-time factor permits.

The pseudo-code for the OCP is presented in Algorithm 1:

IV. EXPERIMENT DESIGN

To assess the efficacy of the trajectory planning algorithm in reducing MS, experiments need to be performed to

Algorithm 1 NL-OCP for MSM Drive

choose $s_0 = 0, s_f = end\ distance$

Input: $\mathbf{x}_0, \mathbf{x}^{\text{guess}}, \mathbf{u}^{\text{guess}}, w_m, w_t, s_0, s_f, \kappa(s) \forall s_0 \rightarrow s_f$

while $k + N_c \leq s_f$ **do**

$\forall\ k \rightarrow k + N_c$

Calculate: cost function using Equation 8

Solve: OCP using Equations 14-17

Find: $u_{opt}\ minimise\ J$

Calculate: $\mathbf{x}(k \xrightarrow{u} k + N_c)$ with u_{opt} with Equation 12

Update: $\mathbf{x}_0$=**x**, $\mathbf{x}^{\text{guess}}$, $\mathbf{u}^{\text{guess}}$

Shifting window: $k = k + 1$

end while

Return NL-OCP solution : states and control inputs (**x**,**u**)

Display v_x,a_x, a_y, s_n, MSDV, travel time for MSM drive

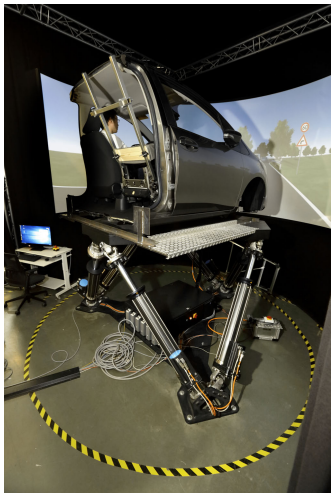

Fig. 3. Delft advanced vehicle simulator.

subjectively assess the occupants' MS levels. In this direction, a driving simulator is employed and human participants are tested regarding the accumulated MS levels using different driving styles. This section entails the design of the experiment and presents the justification for using the selected settings.

A. Apparatus

1) Driving Simulator: Delft Advanced Vehicle Simulator (DAVSi, Figure 3) is used for assessing the effectiveness of optimal trajectories obtained from the proposed algorithm, in the mitigation of motion sickness via human-in-the-loop experiments. DAVSi is a 6-DoF motion platform driving simulator [30], capable of generating acceleration up to 1 g in all directions and can simulate motions in the wide frequency range up to 10 Hz. The half-car Toyota Yaris mock-up with a controllable interface via CAN (levers, buttons, air-con, etc.) is used and extended by the control loading system to provide haptic feedback. The simulator is operated in hard real-time using a dSPACE Scalexio system.

A high-fidelity vehicle model in IPG CarMaker is used to simulate the optimal solutions obtained from the algorithm. The high-fidelity vehicle model, which is the digital twin of the Toyota Yaris, was parameterized using mass-inertia parameters obtained from a vehicle inertia measuring facility.

TABLE II
MOTION & ACTUATORS CONSTRAINTS

Quantity	Lower limit	Upper limit
Longitudinal velocity (v_x)	$3\,\text{m/s}$	$40\,\text{m/s}$
Longitudinal acceleration (a_x)	$-1.5\,\text{m/s}^2$	$1.5\,\text{m/s}^2$
Lateral acceleration (a_y)	$-4\,\text{m/s}^2$	$4\,\text{m/s}^2$
Longitudinal jerk (J_x)	$-1\,\text{m/s}^3$	$1\,\text{m/s}^3$
Deviation from road centre line (s_n)	$-2\,\text{m}$	$2\,\text{m}$
Rate of road wheel angle (d_δ)	$-0.22\,\text{rad/s}$	$0.22\,\text{rad/s}$
Road wheel angle (δ)	$-0.52\,\text{rad}$	$0.52\,\text{rad}$
Yaw rate (r)	$-0.1\,\text{rad/s}$	$0.1\,\text{rad/s}$

The suspension kinematics and compliance were measured on a Kinematics and Compliance test rig for wheel suspension characterization, and finally, validated using field tests by Toyota.

B. Driving Scenario

To investigate the sickness of the participants within a limited time of 45 min, an accelerated sickening road path is designed providing high magnitude sickening stimuli. The design of this road path can be found in Appendix A. The path consists of abundant curves and corners eliciting sickening lateral accelerations within the curvy sections. Along with the lateral acceleration, the vehicle also decelerates before the curve and accelerates after exiting the curve. This reduces lateral acceleration, but increases longitudinal sickening stimuli. The sickening path is designed with a limited lateral displacement to better (but not completely) fit the motion range of the driving simulator.

In the OCP described in section III, the desired path is defined using its curvilinear co-ordinates, distance and curvature. Additionally, the operational driving limits were restricted to comply with highway driving. Along with these driving limits, several constraints related to comfort and actuators were introduced (Table II). Limits on lateral deviation were defined to offer the vehicle lateral maneuverability and help the algorithm to find a better path for MS mitigation, while staying within the road boundaries.

The travel time and the MSDV vary with the change in weights on their cost terms, w_m and w_t. Considering the restriction on experiment duration of 45 min, the trade-off between the accumulated MSDV over the journey, and the distance travelled was analysed for different configurations of the ratio w_m/w_t (see Figure 4). As the solution remains invariant when both weights w_m and w_t are scaled with the same factor, only the ratio w_m/w_t affects the results. Based on Figure 4, an increase in the distance travelled results in high MSDV. Since every individual is differently susceptible towards MS [31], there are no unique settings suitable for all passengers. Different settings can be used in accordance with the occupant's preference. In this study, we further selected settings represented by the larger black dot in Figure 4 which results in around 60% reduction of MSDV, when compared to the least MS mitigating setting (red dot in Figure 4) from the simulated cases. The selected settings resulted in an MSDV of $34\,\text{m/s}^{1.5}$ and travel distance of 16.7 km. This setting was chosen for the MSM drive in the following analysis.

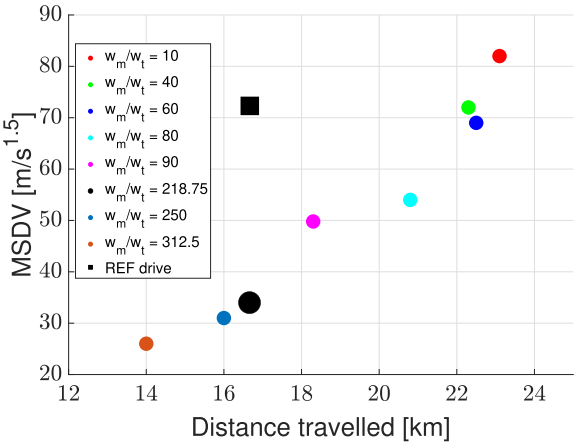

Fig. 4. Effect of OCP cost function weight factor on MSDV and travel distance. Dots represent OCP results where the large black dot represents the selected MSM drive. The square represents the more aggressive reference drive.

C. Reference Driving Style

To compare the effectiveness of the proposed algorithm in reduction of MS, a benchmark case has been defined based on the driver model used in IPG CarMaker [32]. For the longitudinal control, the artificial driver model (aggressive driving with a speed limit of 40 m/s) is used, coupled with path-following lateral control. From here on, the benchmark algorithm will be referred to as '*reference automation drive*' (REF drive). The acceleration limits are kept the same as in the MSM drive, to create a dynamic yet not overly aggressive driving style.

The resultant MSDV for the REF case is 72.7 m/s^2, which is higher than the selected settings for MSM drive, but 12% lower when compared to the least MS mitigating setting (red dot in Figure 4) from the simulated cases. The REF drive is also 1.5 times faster in completing the journey.

D. Motion Cueing Tuning

The moving-base simulator has a limited workspace envelope. Therefore, a motion cueing algorithm (MCA) is adopted and the MCA parameters were tuned to utilise the workspace of the simulator as much as possible, but at the same time ensuring that the workspace limits are not violated. Maximum utilisation of simulator workspace results in a higher motion range and corresponding motion sickening stimuli. To that end, an adaptive washout filter was used for motion cueing; as this filter is known to be more effective in terms of reducing false cueing [33]. Various gains and cut-off frequencies for fore-aft and sway motion have been explored to maximise workspace utilisation and to obtain the maximum sickening stimuli (Table III). According to Table III, with setting 3, the simulator realises the highest MSDV of 17.1 which is around 50% of the MSDV resulting from the actual vehicle acceleration. However, setting 3 obtains a much higher MSDV as compared to setting 6 which applies a quite common 50% motion scaling allowing a larger motion bandwidth. In both REF drive and MSM drive, the same motion cueing parameters are adopted for a uniform comparison.

To verify the simulator capability for recreation of the desired accelerations, power spectral analysis of the accelerations was performed (Figure 6 and Figure 7). According to Figure 6, the longitudinal acceleration power spectra for the virtual vehicle and the driving simulator overlap after 0.25 Hz. Similarly, based on Figure 7, the lateral acceleration power spectrum for the simulator and the virtual vehicle are fairly close beyond 0.2 Hz. Based on these figures, motions beyond 0.2 Hz are sufficiently replicated with the selected motion cueing algorithm parameters.

TABLE III
MOTION CUEING PARAMETERS

Setting	Cut-off frequency (rad/s)	Gain	MSDV
1	2	0.9	12.1
2	1	0.9	15.54
3	1	1	17.1
4	0.5	0.8	15.4
5	0.4	0.5	16.2
6	0.5	0.5	10.4

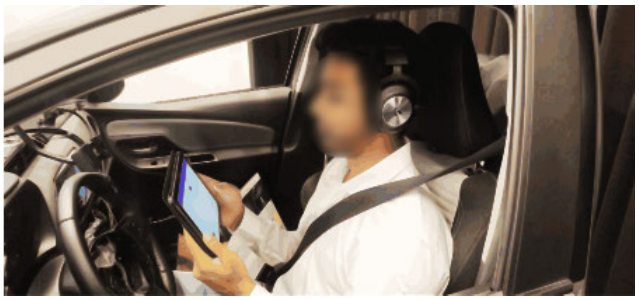

Fig. 5. Participant performing the non-driving task in the simulator.

E. Experimental Procedure

All participants gave informed consent before participation. The Human Research Ethics Committee of TU Delft, Netherlands approved the experiment protocol under application number 1675.

In total, 16 participants from the pool of students and employees of TU Delft participated in the study (mean age: 24.9, std: 1.61 years, 1 female, 15 males). All participants were subjected to both MSM and REF drive. To avoid habituation [34] to the simulator motions, there was at least a week's gap between the two sessions for any participant. Additionally, for the same reason, half the participants were subjected to the MSM drive first and the rest to the REF drive first. Before the initiation of the experiment, the participants were given a safety briefing, which was then followed by the motion sickness susceptibility questionnaire (MSSQ). This questionnaire gives information on the susceptibility of an individual towards getting motion sick. Two-way communication between the researchers and the participants was established via blue-tooth headphones and microphones. Although the participants were not intended to reach retching, sick bags were positioned within easy reach. The participants were also instructed to not consume food at least two hours before the experiment.

As soon as the participants were ready to start the experiment, they were driven in fully automated mode for 45 min in case of MSM drive and 30 min in case of REF drive. The distance travelled in both drive cases was kept constant (16.7 km), resulting in a longer duration for the MSM drive,

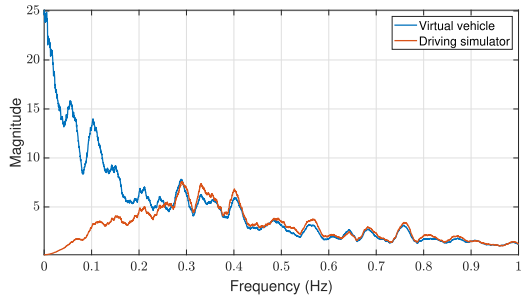

Fig. 6. Longitudinal acceleration in the virtual vehicle and the driving simulator for MSM drive.

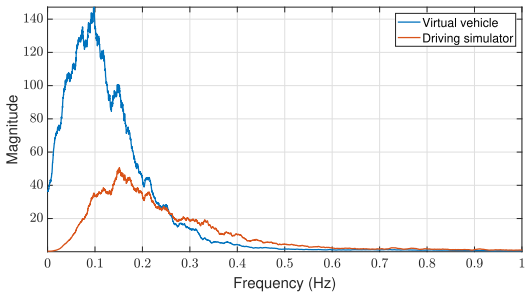

Fig. 7. Lateral acceleration in the virtual vehicle and the driving simulator for MSM drive.

enabling a fair comparison between the accumulated sickness over the trip for the two driving styles. During the driving session, the participants performed a non-driving task, answering a simple yes/no question quiz on a tablet. During the non-driving activity, the participants were instructed to place the tablet in front of them, around chest level, while operating it (see Figure 5). They were also asked to not look out of the simulator, resulting in 'internal vision' (eyes-off-the-road), which is a representative scenario for automated driving.

During the experiment, sickness ratings were queried based on the 11-point subjective MIsery SCale (MISC) [35] in 30 s intervals and their verbal responses were recorded. If the participant reached a MISC level of 6, the experiment was terminated, because this level corresponds to the inception of slight nausea and is deemed an appropriate threshold as observed in pilot runs. Upon the completion of an experimental session, the participants filled out the Motion Sickness Assessment Questionnaire (MSAQ). In this questionnaire, the participant rated the severity of experienced symptoms of MS in detail, at the end of the experimental session.

V. Results

A. Optimal Trajectory Planning

1) Velocity and Path Profile: The optimal velocity and path for a small section of the path is presented in Figure 8. According to the figure, the velocity for the displayed part of the path ranges from 5 m/s to 10 m/s, and between 5 m/s and 6 m/s for the REF drive and the MSM drive, respectively. Similarly, for the entire journey (road path), the velocity ranges from 5 m/s to 22 m/s, and between 3 m/s and 10 m/s for the REF drive and the MSM drive, respectively. The REF drive executes a limited reduction in its velocity while approaching the corners. Whereas, in case of MSM drive, the vehicle slows down to velocities near 3 m/s (lowest allowed velocity). Moreover, the MSM drive does not follow the center-line of the path and cuts the corners within the selected limits, to reduce the lateral acceleration. This driving behavior provides a more suitable path for reducing the motion sickening stimuli.

2) Acceleration: The G-G diagram obtained from the simulation is presented in Figure 9. The blue and the red dots depict the acceleration achieved through the REF and the MSM drive, respectively. Based on the figure, higher longitudinal accelerations are achieved in the REF drive, whereas the lateral acceleration ranges are similar in both drives. Furthermore, Figure 9 shows that higher accelerations have a lower occurrence in the MSM drive rather than in the REF drive. Occasionally the defined acceleration constraints are violated in the MSM drive. The latter occurs as the optimal solution is obtained using a 3-DOF vehicle model, but the G-G diagram is extracted after simulating the optimal solution with a high-fidelity vehicle model. Due to the low occurrence of high amplitude accelerations, the MSDV obtained for the MSM drive is 34 $m/s^{1.5}$, whereas the MSDV obtained for the REF drive is 72.7 $m/s^{1.5}$. This indicates a significant decrease in motion sickening stimuli.

3) Lateral Deviation: The proposed algorithm was analyzed for the effect of allowed lateral deviation from the road lane centre. The cases considered were from 0.5 to 2 m with steps of 0.5 m. No values lower than 0.5 m were considered, as constraining the lateral deviation to a lower value resulted in infeasible optimisation at some stages (horizons of the sliding window). A possible reason for this occurrence is the complexity of the path, for which the solver could not converge to a feasible solution that follows the path without violating the constraints.

According to Table IV, when the allowed lateral deviation was increased, the MSDV through the whole path reduced. Moreover, the travel time reduced with increased lateral deviation; as corner cutting allows the vehicle to continue at slightly higher velocities (as the lateral accelerations reduce with corner cutting) and also reduces the actual overall distance travelled marginally. Specifically, when the lateral deviation was increased from 0.5 m to 1 m the MSDV reduced by 19.25%. Increasing it further from 1 m to 1.5 m, the MSDV reduced by 6.78%, and finally from 1.5 m to 2 m, the reduction in MSDV was 3.38%. This illustrates that the initial increment in the lateral deviation has the highest impact on MS reduction, and as the lateral deviations are increased further the impact on MS mitigation reduces.

Regarding the travel time, it also showed decrements with the increase of lateral deviation. Particularly, when the lateral deviation was increased from 0.5 m to 2 m the travel time reduced by 15.6%. Increasing it from 0.5 m to 1 m reduced the travel time by just 3.96%. Increasing it further from 1 m to 1.5 m reduced the travel time by 8.45% and lastly, increasing it from 0.5 m to 2 m reduced the travel time by 4.08%.

B. Driving Simulator Validation

1) Realised Accelerations: Figure 10 shows the G-G diagram for the accelerations realised in the driving simulator. According to Figure 9 and Figure 10, the accelerations attained by the two drives are lower in magnitude inside the simulator,

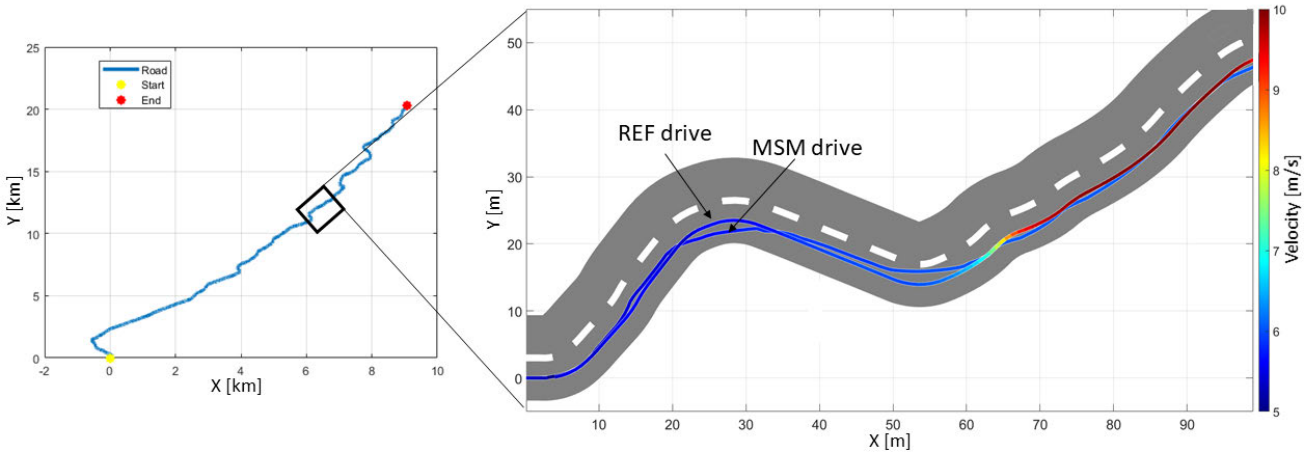

Fig. 8. Trajectories of MSM drive and REF drive for a small section of the path.

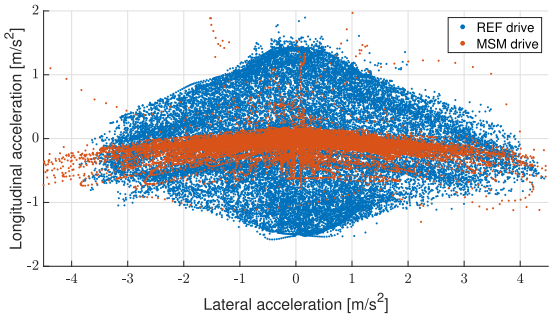

Fig. 9. G-G diagram of the virtual vehicle acceleration achieved for REF and MSM drive.

TABLE IV

EFFECTS OF ALLOWED LATERAL DEVIATION FROM THE ROAD CENTER LINE ON MSDV AND TRAVEL TIME

Allowed deviation	MSDV	Travel time
0.5 m	46.74 m/s$^{1.5}$	53.0 min
1.0 m	37.75 m/s$^{1.5}$	50.9 min
1.5 m	35.19 m/s$^{1.5}$	46.6 min
2.0 m	34.0 m/s$^{1.5}$	44.7 min

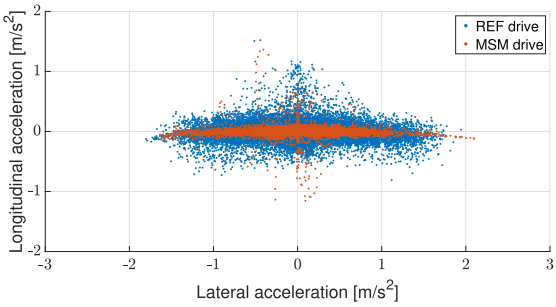

Fig. 10. G-G diagram of the simulator platform acceleration realised in the driving simulator for REF and MSM drive.

which is expected due to limited simulator workspace. However, based on Figure 6 and Figure 7, the power is reduced below 0.2 Hz, but is replicated fairly beyond that point. Thus, the selected MCA parameters retain motion characteristics above 0.2 Hz in the applied driving simulator motion.

2) Participants' Sickness Levels: General motion sickness susceptibility assessed prior to the experiment yielded a mean MSSQ of 17.14 with a standard deviation of 10.03 over the selected participants. This mean translates to a percentile of 69%, which indicates that our participants have a slightly above-average motion sickness susceptibility. The standard deviation translates to 52.94% to 81.49% percentiles, indicating that our participants cover a reasonable range of susceptibility.

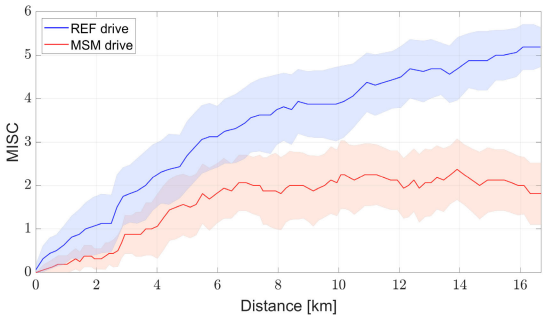

Fig. 11. Mean MISC scores for MSM and REF drive.

For the MSM drive only one participant dropped out reaching MISC level of 6, whereas in case of REF drive 7 out of 16 participants dropped out of the experiment. Hence, the algorithm was effective in motion planning to reduce the amount of participants stopping the experiment approaching retching levels. The mean MISC scores representing the sickness levels of the participants are shown in Figure 11. The blue line depicts the mean MISC for the REF drive, whereas the red line shows the mean MISC for the MSM drive. The shaded areas around the plotted lines depict the standard deviation of MISC ratings for the participants. It should be noted that, in cases of a participant stopping the experiment, their MISC score was considered to be 6 till the end of the experiment for the calculation of mean MISC (in practice it should rise further).

According to Figure 11, the MSM drive is less sickening during the entire journey. In fact, the mean MISC value at the end of the experiment for MSM drive is 65% lower compared to REF drive. Overall, the participants showed a very high variability in the MISC scores during the experiment due to their motion sickness susceptibility. Even with this variability in the MISC scores, all the participants had reduced sickness levels when they were subjected to MSM drive, compared to REF drive (Figure 13 in Appendix B).

TABLE V
DISTANCE TRAVELLED BY PARTICIPANTS BEFORE REACHING SPECIFIC MISC LEVELS

MISC level	AV driving style	Mean distance (std), km
1	MSM drive	2.8 (1.83)
	REF drive	1.52 (1.29)
2	MSM drive	6.3 (4.21)
	REF drive	3.14 (2.01)
3	MSM drive	6.91 (2.82)
	REF drive	4.47 (2.04)

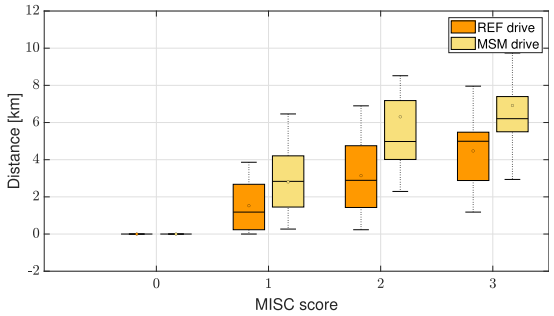

Fig. 12. Boxplot of onset of the levels of motion sickness with respect to distance travelled.

The onsets of increasing motion sickness levels were analysed through boxplots in Figure 12. The onsets up to MISC level of 3 are provided, as, with the MSM drive, not many participants reached a MISC level beyond 3. This is another indication of the algorithm's ability to successfully mitigate motion sickness. Furthermore, the mean distance travelled before a participant reaches a specific MISC level and its standard deviation are given in Table V. This shows that the distance travelled by the participants before reaching each and every MISC level is more in case of MSM drive compared to REF drive.

Along with the continuous MISC measurements during the experiment, post experiment MSAQ ratings were collected. For REF drive the mean MSAQ for all the participants was 65.56 with a standard deviation of 18.91, whereas, for MSM drive, the mean MSAQ for all the participants was 37.69 with a standard deviation of 17.71. All the participants reported a reduced MSAQ score with MSM drive. The results of the single-tailed t-test ($p = 4.9e-4$) on this dataset confirm the assertion that the algorithm effectively mitigates MS.

Finally, the general sickness susceptibility using MSSQ prior to the experiment was evaluated in relation to the actual sickness. Based on Table VI, the correlation of MSSQ with any of the sickness indicators is not significant. This implies that MSSQ is not a reliable metric to predict the susceptibility of an individual to motion sickness in the conditions tested. This is coherent with [36] reporting a moderate correlation with MSSQ ($\rho = 0.5$, $p = 0.05$) in 0.3 Hz fore-aft motion.

VI. DISCUSSION

The effectiveness of the optimal trajectory planning for mitigating MS has been evaluated. This was conducted by comparing the optimal MSM drive with REF drive (baseline) in human-in-the-loop experiments using a moving-base driving simulator.

TABLE VI
CORRELATION COEFFICIENTS BETWEEN MSSQ SCORES AND DIFFERENT SICKNESS INDICATORS AND THEIR RESPECTIVE P-VALUES

Data-set	Correlation coefficient	p-value
Max MISC: MSM drive case	0.3493	0.1849
Max MISC: REF case	0.1877	0.4864
MSAQ: MSM drive case	0.3623	0.1679
MSAQ: REF case	0.4349	0.0922

In MSM drive, the vehicle reduces its velocity during the corners, leading to decreased lateral accelerations that a passenger is subjected to. This is a desired behaviour to reduce the sickening stimuli. The algorithm also modifies the pre-defined path allowing the vehicle to perform corner cutting. Such adjustments to the path led to a further reduction in lateral acceleration, since corner cutting increases the turning radius. This renders the ride more comfortable and less sickening.

The G-G diagram in Figure 9 indicates a large reduction in longitudinal and lateral accelerations in MSM drive. The objective of the algorithm is to minimise MSDV; hence, the algorithm limits the velocity reduction in cornering, attaining a higher lateral acceleration, but limiting the longitudinal deceleration. This results in a lower overall MSDV.

For the selected weight settings, the MSDV for the journey reduced by 53% with the proposed MSM algorithm. This aligns with the projections made in the literature [22], [23], as expected due to the presence of MSDV in the cost function. According to Figure 4 as the weight ratio w_m/w_t is increased, the MSDV through the journey reduces. Moreover, as MSDV minimization reduces the vehicle velocities/accelerations, a very high ratio of the weight, w_m/w_t, would result in an optimal solution with very low velocities, which are preferable for MS mitigation. However, the excessive reduction of velocity leads to the occupants' dissatisfaction [37], [38]; as the journey time will be too long, violating their expectation for travelling long distances in a short period of time. An alternative would be to prompt users to watch the road during sickening road sections, and avoid engagement in non-driving tasks.

The experimental study in the driving simulator was conducted to gauge the effectiveness of the proposed method in reducing MS using human beings. The recent state-of-the-art studies for MS mitigation assess their proposed algorithms only via simulations and lack experimental validation with humans. The experiments in this study demonstrate that the proposed algorithm is effective in reducing experienced motion sickness with human participants across a substantial range of individual susceptibility. In general, our results are in line with the simulation studies mentioned earlier. Regarding the efficiency of the driving simulator, the accelerations (Figure 6 and Figure 7) beyond 0.2 Hz were replicated closely in the driving simulator, whereas the accelerations below that frequency could not be captured due to the limited workspace of the simulator. Although the range of frequency for human susceptibility to motion sickness is from 0.1 Hz to 0.8 Hz, the tuned settings of the simulator allowed us to replicate the frequency range beyond 0.2 covering a large part of the focus range.

Regarding the experiment, an accelerated sickening path was used to seek the optimal solution and subjectively test the occupants' motion sickness levels. During the experiment, only one participant dropped out when the proposed algorithm was used, i.e. in MSM drive. Meanwhile, even this participant travelled a longer distance until dropping out compared to the REF drive. This indicated that the algorithm had a positive effect on MS mitigation for each and every individual, when compared to the REF drive which tries to follow the lane center and is not close to human-like negotiating curves. Our proposed algorithm is expected to outperform any human-like driving algorithm since it optimises both velocity and path for the mitigation of MS. However, such comparison is considered as scope for future study. The proposed algorithm suffers from certain limitations as well. All the participants showed differing MS susceptibility during the experiment. Thus, there is no single weight setting for the cost function that would suit the entire population. Weight sets need to be defined for different individuals or different susceptibility groups. We recommend performing user groups studies to assess if different comfort pre-sets would provide a benefit to more people.

The algorithm also makes a trade-off between the travel time and sickness reduction, which adheres to the findings from [23]. In the conducted experiment, the travel time of the journey increased by 50% with mitigation of MS. The road profile used for the experiment was high on sickening stimuli. For paths with lower sickening stimuli as occurring in many highways, the vehicle velocity will often be constrained by speed limits, and hence the travel time increase will be limited.

VII. Conclusion

Trajectory planning for mitigation of motion sickness in automated vehicles through optimal control has been proposed. The algorithm outputs a comfortable reference velocity profile. Moreover, it generates a preferred path through corner cutting within the allowable road area. This allows the vehicle to corner with lower lateral acceleration reducing the sickening motion stimuli.

The effectiveness of the proposed algorithm in reduction of motion sickness was studied using a driving simulator experiment. The proposed algorithm successfully reduced the levels of motion sickness for the 16 participants, where, the mean MIsery SCale scores reported by the participants reduced by 65% compared to the benchmark controller. Each and every participant reported reduced levels of sickness, when subjected to the proposed driving style, and the number of dropouts reduced from 6 to 1. The overall journey was also rated as more comfortable by the participants, indicated by a 57.48% reduction in the mean score of Motion Sickness Assessment Questionnaire, which confirms the algorithm's capability in reduction of motion sickness in each and every individual.

Although all participants reported reduced motion sickness with the proposed algorithm, the individual sickness levels displayed a substantial variance. This calls for subject-specific comfort settings in automated vehicles.

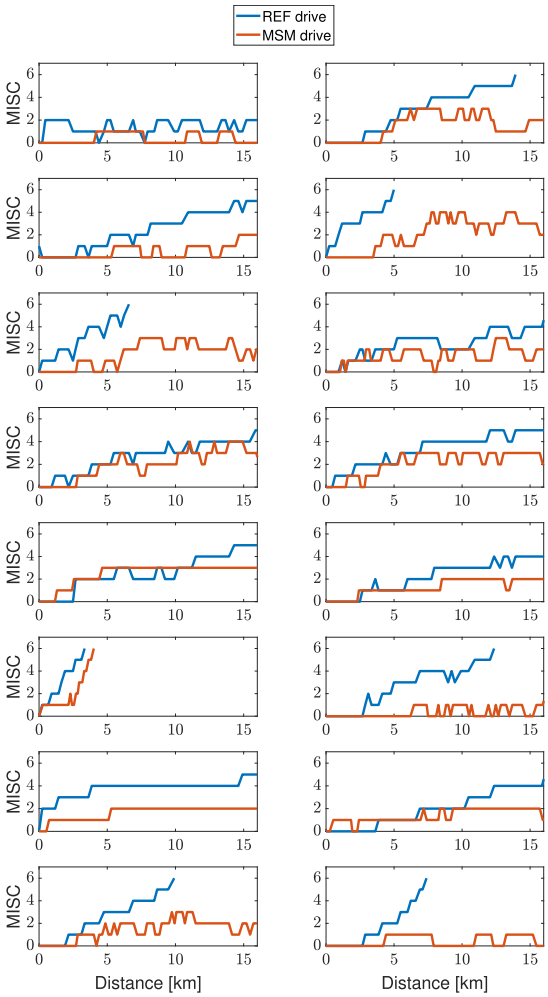

Fig. 13. Individual MISC scores for all the participants.

Appendix A
Accelerated Sickening Path Design

The objective of the road generation is to extract the maximum sickening stimuli out of the road path.

The inputs that the optimisation chooses to maximise the MSDV are a_x and β i.e. the longitudinal acceleration and the side slip angle. The overall algorithm for the path optimisation is:

$$\max_{u \in U} \; MSDV \tag{18}$$

$$s.t.: \; Ax' = f(x, u, s) \tag{19}$$

$$u_{min} \leq u(k) \leq u_{max} \tag{20}$$

$$x_{min} \leq x(k) \leq x_{max} \tag{21}$$

where, Equation 20 and Equation 21 define the constraints to the inputs and the states of the model in the optimal control problem.

The equations of motion for the vehicle model used for the road generation in Equation 19, are presented below:

$$\dot{v_x} = a_x + \dot{\psi} v_y \tag{22}$$

$$\dot{v_y} = \dot{\psi} v_x \tag{23}$$

$$\dot{X} = V \; cos(\psi + \beta) \tag{24}$$

$$\dot{Y} = V \; sin(\psi + \beta) \tag{25}$$

TABLE VII

Parameter	Value
Algorithmic differentiation tool	CasADi 3.5.1
Prediction horizon for the sliding window	100 m
Step size	1 m
Shifting step size (Sliding window)	1 m
Integrator	ERK4
Integrator nodes	5
Solver method	PDIP NLP
Solver maximum iterations	2000
Tolerance	10^{-6}

TABLE VIII

Annotation	Description	Unit
AVs	Automated vehicles	-
a_x	Longitudinal vehicle acceleration in local frame of reference	m/s^2
$a_{x,w}(t)$	Frequency-weighted longitudinal acceleration	m/s^2
a_y	Lateral vehicle acceleration in local frame of reference	m/s^2
$a_{y,w}(t)$	Frequency-weighted lateral acceleration	m/s^2
$C_{\alpha f}$	Cornering stiffness of the front tyres	N/rad
$C_{\alpha r}$	Cornering stiffness of the rear tyres	N/rad
f_v	Function defining the nonlinear state space relation	-
g	Acceleration due to gravity	m/s^2
I_z	Moment of inertia of the vehicle about vertical axis	kgm^2
J_c	Cost function for the optimal control problem	-
J_x	Longitudinal jerk in vehicle's local frame of reference	m/s^3
k	Current simulation step	-
L_f	Distance of front axle from the vehicle COG	m
L_r	Distance of rear axle from the vehicle COG	m
m	Mass of the vehicle	kg
MISC	MIsery SCale (Subjective motion sickness rating scale)	-
MS	Motion sickness	-
MSAQ	Motion sickness assessment questionnaire	-
MSDV	Motion sickness dose value	$m/s^{1.5}$
MSM-drive	Motion sickness mitigation drive (proposed algorithm)	-
N_c	Length of the control horizon/ shifting horizon window	-
OCP	Optimal control problem	-
p	Generalised parameter	-
p'	Partial derivative of the generalised parameter w.r.t. space	-
s	Distance travelled by the vehicle	m
r	Vehicle yaw rate	rad/s
REF-drive	Reference automation drive (benchmark driving style)	-
s_0	Start-point of the road	m
s_f	End-point of the road	m
s_n	Lateral deviation of the vehicle from the lane center-line	m
T	Travel time	s
u	Control inputs (J_x and d_δ)	-
u^{guess}	Initial guess for the optimised inputs of the OCP	-
u_{opt}	Optimal control input	-
v_x	Longitudinal vehicle velocity in local frame of reference	m/s
v_y	Lateral vehicle velocity in local frame of reference	m/s
w_m	Weighting coefficient for MSDV in the cost function	-
w_t	Weighting coefficient for travel time in the cost function	-
x^{guess}	Initial guess for the states of the OCP	-
x_v	Vehicle states	-
α	Deviation of the vehicle heading angle from the road heading	rad
d_δ	Rate of change of steering wheel angle	rad/s
δ	Steering angle	rad
κ	Curvature of the road	m^{-1}
μ	Friction coefficient of the road	-
θ	Road heading angle	rad
ψ	Vehicle heading angle	rad

$$\dot{s} = V \tag{26}$$

$$\dot{\psi} = \frac{V}{L}\ cos(\beta)\ tan(\delta) \tag{27}$$

$$a_x = a\ cos(\psi) \tag{28}$$

$$a_y = a\ sin(\psi) \tag{29}$$

$$V = \sqrt{{v_X}^2 + {v_y}^2} \tag{30}$$

$$\delta = tan^-1\left(\frac{\beta L}{l_r}\right) \tag{31}$$

where, V is the vehicle velocity; X and Y are the longitudinal and lateral positions in the global frame of reference; β is the side slip angle, and ψ is the heading angle; L is the wheelbase.

The vehicle model is allowed to take any actions within the specified limits, that make the movement feasible for a real vehicle according to the constraints in Table II. A constraint is added on the local lateral displacements of the vehicle as well. This local lateral displacement limit is added considering the full workspace limit of the driving simulator (1 m). It shall be noted that the actual lateral displacement (see Figure 8) is larger due to vehicle yaw rotation.

The optimisation outputs a set of longitudinal acceleration and sideslip angle data to achieve maximum MSDV. Through this data and the initial conditions, all the states can be calculated. As the aim of this work is to obtain the accelerated sickening road path, the longitudinal and lateral distances (X and Y as described in equations 24 and 25) in global frame of reference are calculated and recorded. The sickening path is shown in Figure 8.

The obtained MSDV for this road profile is $99 m/s^{1.5}$ with a total span of the road being 25.3 km.

APPENDIX B
INDIVIDUAL MISC RESPONSES

See Fig. 13.

APPENDIX C
SOLVER SETTINGS

See Table VII.

APPENDIX D
NOMENCLATURE TABLE

See Table VIII.

REFERENCES

[1] M. Martínez-Díaz, F. Soriguera, and I. Pérez, "Autonomous driving: A bird's eye view," *IET Intell. Transp. Syst.*, vol. 13, no. 4, pp. 563–579, Apr. 2019.

[2] T. Litman, "Autonomous vehicle implementation predictions: Implications for transport planning," Victoria Transp. Policy Inst. Victoria, Victoria, BC, Canada, Tech. Rep., 2020. [Online]. Available: https://www.vtpi.org/avip.pdf

[3] I. Pettersson and I. C. M. Karlsson, "Setting the stage for autonomous cars: A pilot study of future autonomous driving experiences," *IET Intell. Transp. Syst.*, vol. 9, no. 7, pp. 694–701, Sep. 2015.

[4] D. Paddeu, G. Parkhurst, and I. Shergold, "Passenger comfort and trust on first-time use of a shared autonomous shuttle vehicle," *Transp. Res. C, Emerg. Technol.*, vol. 115, Jun. 2020, Art. no. 102604.

[5] C. Diels and J. E. Bos, "Self-driving carsickness," *Appl. Ergonom.*, vol. 53, pp. 374–382, Mar. 2016.

[6] B. Paden, M. Cáp, S. Z. Yong, D. Yershov, and E. Frazzoli, "A survey of motion planning and control techniques for self-driving urban vehicles," *IEEE Trans. Intell. Vehicles*, vol. 1, no. 1, pp. 33–55, Mar. 2016.

[7] A. Scheuer and T. Fraichard, "Continuous-curvature path planning for car-like vehicles," in *Proc. IEEE/RSJ Int. Conf. Intell. Robot Systems. Innov. Robot. Real-World Appl.*, Sep. 1997, pp. 997–1003.

[8] E. Lambert, R. Romano, and D. Watling, "Optimal path planning with clothoid curves for passenger comfort," in *Proc. 5th Int. Conf. Vehicle Technol. Intell. Transp. Syst.*, 2019, pp. 609–615.

[9] I. Bae, J. H. Kim, J. Moon, and S. Kim, "Lane change maneuver based on Bezier curve providing comfort experience for autonomous vehicle users," in *Proc. IEEE Intell. Transp. Syst. Conf. (ITSC)*, Oct. 2019, pp. 2272–2277.

[10] D. Gonzalez, V. Milanes, J. Perez, and F. Nashashibi, "Speed profile generation based on quintic Bezier curves for enhanced passenger comfort," in *Proc. IEEE 19th Int. Conf. Intell. Transp. Syst. (ITSC)*, Nov. 2016, pp. 814–819.

[11] K. N. de Winkel, T. Irmak, R. Happee, and B. Shyrokau, "Standards for passenger comfort in automated vehicles: Acceleration and jerk," *Appl. Ergonom.*, vol. 106, Jan. 2023, Art. no. 103881.

[12] A. Artuñedo, J. Villagra, and J. Godoy, "Jerk-limited time-optimal speed planning for arbitrary paths," *IEEE Trans. Intell. Transp. Syst.*, vol. 23, no. 7, pp. 8194–8208, Jul. 2022.

[13] M. B. Loknar, S. Blažic, and G. Klancar, "Minimum-time velocity profile planning for planar motion considering velocity, acceleration and jerk constraints," *Int. J. Control*, vol. 96, no. 1, pp. 251–265, Jan. 2023.

[14] H. Shin, D. Kim, and S. Yoon, "Kinodynamic comfort trajectory planning for car-like robots," in *Proc. IEEE/RSJ Int. Conf. Intell. Robots Syst. (IROS)*, Oct. 2018, pp. 6532–6539.

[15] Y. Zheng, B. Shyrokau, and T. Keviczky, "Comfort and time efficiency: A roundabout case study," in *Proc. IEEE Int. Intell. Transp. Syst. Conf. (ITSC)*, Sep. 2021, pp. 3877–3883.

[16] F. Hegedus, T. Bécsi, S. Aradi, and P. Gápár, "Model based trajectory planning for highly automated road vehicles," *IFAC-PapersOnLine*, vol. 50, no. 1, pp. 6958–6964, Jul. 2017.

[17] J. Ziegler, P. Bender, T. Dang, and C. Stiller, "Trajectory planning for bertha—A local, continuous method," in *Proc. IEEE Intell. Vehicles Symp.*, Jun. 2014, pp. 450–457.

[18] X. Qian, I. Navarro, A. de La Fortelle, and F. Moutarde, "Motion planning for urban autonomous driving using Bezier curves and MPC," in *Proc. IEEE 19th Int. Conf. Intell. Transp. Syst. (ITSC)*, Nov. 2016, pp. 826–833.

[19] R. Lattarulo and J. P. Rastelli, "A hybrid planning approach based on MPC and parametric curves for overtaking maneuvers," *Sensors*, vol. 21, no. 2, p. 595, Jan. 2021.

[20] D. Li and L. Chen, "Mitigating motion sickness in automated vehicles with vibration cue system," *Ergonomics*, vol. 65, no. 10, pp. 1313–1325, Oct. 2022.

[21] D. Li, B. Xu, L. Chen, and J. Hu, "Automated car-following algorithm considering passenger motion sickness," in *Proc. Int. Symp. Future Act. Saf. Technol. Toward Zero Traffic Accidents*, 2021, pp. 1–6.

[22] C. Certosini, R. Capitani, and C. Annicchiarico, "Optimal speed profile on a given road for motion sickness reduction," 2020, *arXiv:2010.05701*.

[23] Z. Htike, G. Papaioannou, E. Siampis, E. Velenis, and S. Longo, "Fundamentals of motion planning for mitigating motion sickness in automated vehicles," *IEEE Trans. Veh. Technol.*, vol. 71, no. 3, pp. 2375–2384, Mar. 2022.

[24] D. Li and J. Hu, "Mitigating motion sickness in automated vehicles with frequency-shaping approach to motion planning," *IEEE Robot. Autom. Lett.*, vol. 6, no. 4, pp. 7714–7720, Oct. 2021.

[25] T. Irmak, D. M. Pool, and R. Happee, "Objective and subjective responses to motion sickness: The group and the individual," *Exp. Brain Res.*, vol. 239, no. 2, pp. 515–531, Feb. 2021.

[26] *Mechanical Vibration and Shock-evaluation of Human Exposure to Whole Body Vibration. Part 1: General Requirements*, Int. Org. Standardization (ISO), Geneva, Switzerland, 1997.

[27] J. Golding, H. Markey, and J. Stott, "The effects of motion direction, body axis, and posture on motion sickness induced by low frequency linear oscillation," *Aviation, Space, Environ. Med.*, vol. 66, no. 11, pp. 1046–1051, 1995.

[28] B. E. Donohew and M. J. Griffin, "Motion sickness: Effect of the frequency of lateral oscillation," *Aviation, Space, Environ. Med.*, vol. 75, no. 8, pp. 649–656, 2004.

[29] A. Domahidi and J. Jerez. (2014). *Forces Professional*. Embotech GMBH. [Online]. Available: http://embotech.com/forces-pro

[30] Y. R. Khusro, Y. Zheng, M. Grottoli, and B. Shyrokau, "MPC-based motion-cueing algorithm for a 6-DOF driving simulator with actuator constraints," *Vehicles*, vol. 2, no. 4, pp. 625–647, Dec. 2020.

[31] T. Irmak, K. N. de Winkel, D. M. Pool, H. H. Bulthoff, and R. Happee, "Individual motion perception parameters and motion sickness frequency sensitivity in fore-aft motion," *Exp. Brain Res.*, vol. 239, no. 6, pp. 1727–1745, Jun. 2021.

[32] B. Alrifaee and J. Maczijewski, "Real-time trajectory optimization for autonomous vehicle racing using sequential linearization," in *Proc. IEEE Intell. Vehicles Symp. (IV)*, Jun. 2018, pp. 476–483.

[33] H. Arioui, L. Nehaoua, and H. Amouri, "Classic and adaptive washout comparison for a low cost driving simulator," in *Proc. IEEE Int. Symp. Mediterrean Conf. Control Autom. Intell. Control*, 2005, pp. 586–591.

[34] N. Duzmanska, P. Strojny, and A. Strojny, "Can simulator sickness be avoided? A review on temporal aspects of simulator sickness," *Frontiers Psychol.*, vol. 9, p. 2132, Nov. 2018.

[35] K. N. de Winkel, T. Irmak, V. Kotian, D. M. Pool, and R. Happee, "Relating individual motion sickness levels to subjective discomfort ratings," *Exp. Brain Res.*, vol. 240, no. 4, pp. 1231–1240, Apr. 2022.

[36] T. Irmak, V. Kotian, R. Happee, K. N. de Winkel, and D. M. Pool, "Amplitude and temporal dynamics of motion sickness," *Frontiers Syst. Neurosci.*, vol. 16, pp. 1–15, May 2022, doi: 10.3389/fnsys.2022.866503.

[37] S. Nordhoff, J. de Winter, W. Payre, B. van Arem, and R. Happee, "What impressions do users have after a ride in an automated shuttle? An interview study," *Transp. Res. F, Traffic Psychol. Behaviour*, vol. 63, pp. 252–269, May 2019.

[38] R. Krueger, T. H. Rashidi, and J. M. Rose, "Preferences for shared autonomous vehicles," *Transp. Res. C, Emerg. Technol.*, vol. 69, pp. 343–355, Aug. 2016.

Vishrut Jain received the M.Sc. degree in vehicle engineering from the Delft University of Technology (TU Delft), The Netherlands, in 2019. He is currently pursuing the Ph.D. degree with the Section of Intelligent Vehicles, TU Delft, in collaboration with Toyota Motors Europe, exploring the motion planning aspects and control methods to mitigate motion sickness in automated vehicles and in driving simulators. His research interests include vehicle control, and co-operative and autonomous driving.

Sandeep Suresh Kumar received the M.Sc. degree from the Delft University of Technology, The Netherlands, in 2021. In his M.Sc. thesis, he worked on motion planning algorithm for automated driving. He is currently a Design Engineer in the field of systems and controls with ASML, The Netherlands.

Georgios Papaioannou received the Ph.D. degree from the National Technical University of Athens (NTUA), Greece, in 2019. He is currently an Assistant Professor with the Section of Intelligent Vehicles, Delft University of Technology, after conducting post-doctoral research with the KTH Royal Institute of Technology, Sweden, and Cranfield University, U.K. His research interests include motion comfort, seat comfort, human body modeling, automated vehicles, and optimization and control.

Riender Happee received the Ph.D. degree from the Delft University of Technology (TU Delft), The Netherlands, in 1992. He investigated road safety and introduced biomechanical human models for impact and comfort with TNO Automotive (1992–2007). Currently, he investigates the human interaction with automated vehicles focusing on safety, motion comfort, and acceptance with the Section of Intelligent Vehicles, TU Delft, where he is also a Full Professor.

Barys Shyrokau received the joint Ph.D. degree in control engineering from Nanyang Technological University and the Technical University of Munich in 2015. He is currently an Assistant Professor with the Section of Intelligent Vehicles, Delft University of Technology. His research interests include vehicle dynamics and control, motion comfort, and driving simulator technology. He is the scholarship and award holder of SAE, FISITA, DAAD, SINGA, ISTVS, and CADLM.